Egypt. J. Vet. Sci. **Vol. 55,** No. 1, pp. 157-173 (2024)

Egyptian Journal of Veterinary Sciences
https://ejvs.journals.ekb.eg/

Zinc Oxide Nanoparticles: A Promising Antiviral Therapy of Lumpy Skin Disease Virus in Vitro

Gabr F. El-Bagoury [1], Essam I. El-Toukhy [2], Mohammed G. El-Hamady[2*] and Samr Kassem [3]

[1]*Department of Virology, Faculty of Veterinary Medicine, Benha University, Egypt.*
[2]*Department of Biotechnology, Animal Health Research Institute, Dokki, Agriculture Research Center, Giza, Egypt.*
[3]*Nanomaterials Research and Synthesis Unit, Animal Health Research Institute, Dokki, Agriculture Research Center, Giza, Egypt.*

FIVE nodular samples were collected from clinically suspected cattle for lumpy skin disease (LSD) from five governorates in Egypt during August and September 2020. Real-time PCR confirmed the presence of lumpy skin disease (LSDV) in all samples. One sample was isolated and passaged three times on the chorio-allantoic membrane (CAM) of specific pathogen free embryonated chicken eggs (SPF-ECEs), resulting in the formation of pock lesions. The isolated sample underwent partial gene sequencing of the G-protein coupled chemokine receptor (GPCR) gene for molecular characterization, revealing its close relation to circulating LSDV strains in Africa and the Middle East. Subsequently, zinc oxide nanoparticles (ZnONPs) were synthesised using a green method with zinc sulphate heptahydrate as a precursor and Arabic gum as a stabilizer. Characterization of ZnONPs using Fourier transform spectroscopy (FT-IR), zetasizer, X-ray diffraction (XRD), and transmission electron microscopy (TEM) showed a size range of 23.6 to 38.0 nm and a surface charge of -25.7 mV. The cytotoxicity of ZnONPs was evaluated on human oral epithelial cells (OEC), showing that the survival rate of cells decreased from 100.99 to 90.23% at concentrations of 0.31 and 50 mg/ml respectively. ZnONPs were used to inhibit LSDV replication in Madin Darby bovine kidney (MDBK) tissue culture using plaque reduction assay showing 50% inhibitory concentration (IC50) at 45.36 µg/ml and cytotoxicity (CC50) at 30.9 µg/ml with a selectivity index of 0.68. Furthermore, TEM imaging confirmed the antiviral efficacy of ZnONPs against LSDV. These findings demonstrate the antiviral effect of ZnONPs against LSDV, offering promising applications in veterinary medicine field.

Keywords: LSDV, Real time PCR, GPCR, Antiviral, zinc oxide nanoparticles.

Introduction

Lumpy skin disease (LSD) is a significant infectious disease of cattle that is primarily insect-borne and affects cattle in southern and eastern Africa, as well as more recently in northern Africa and the Middle East [1].

The disease is caused by a *capripoxvirus* (CaPV) of which the prototype strain, "Neethling'" was first isolated in South Africa [2]. Except for Libya, Algeria, Morocco, and Tunisia, LSD is present throughout most of the African countries [3].The first presence of LSD in Egypt was in 1988 in the Suez governorate, then during the summer of 1989 LSD reappeared in 22 of 26 Egyptian governorates [4,5].

During the summer of 1998, an outbreak of LSD occurred among non-vaccinated cattle in El-Menia governorate and Fayoum governorate in Egypt, then another outbreak of LSD occur

*Corresponding author: Mohammed G. El-Hamady, E-mail: dr.m.elhamady@gmail.com. Tel.: 00201060931193
https://orcid.org/0009-0009-9953-2050
(Received 26/06/2023, accepted 18/09/2023)
DOI: 10.21608/EJVS.2023.219490.1530

among cattle in Damietta governorate, Egypt in 2005 [6,7].

LSD is a notifiable disease with great economic importance associated with decreased milk production, loss of weight, poor growth, damage of hide, infertility and abortion [8]. It is characterized by high morbidity and low mortality rates, usually less than 10%, and affects all ages and breeds of cattle [9].

The LSD virion has the rough brick shape and also some viral particles were surrounded by envelop derived from the host cell with the average size of 320-260 nm [10,11]. The lumpy skin disease virus (LSDV) is a DNA virus that has a genome size of 151-kbp. Its genome includes a central coding region flanked by identical 2.4 kbp-inverted terminal repeats, and it is composed of 156 potential genes [12]. LSDV is antigenically and genetically related to the sheep and goat pox viruses (SPV and GPV), and they cannot be differentiated by serological tests but they are phylogenetically distinct and can be differentiated by molecular methods [13]. LSDV infect cattle , but some researches demonstrate the ability of LSDV to infect water buffalo [14].

LSDV is arthropod born disease that is transmitted by Aedes aegypti female mosquitoes, ticks, stable flies and biting midge [15,16]. Despite the virus being present in the nasal, lacrimal, semen, and milk of infected animals, ingestion and direct contact transmission are not common routes of transmission [17].

The cytoplasm is where the LSDV replicates. Viral DNA replication, transcription of viral genes, assembly of infectious viral particles, attachment to host cell membrane, uncoating, release of the virus core, and release via budding or cell lysis are all steps in the viral replication cycle [18].

Most animals develop lifelong cell-mediated immunity to LSDV infection, and calves born to infected cattle get maternal immunity [2].

LSDV incubation period ranged between 2 to 5 weeks and characterized by biphasic fever, enlargement of Superficial lymph nodes and presence of nodules that cover the whole body skin or there may be only a few of them [9]. These nodules can also affect nasal, oral, ocular, and genital mucosa causing Rhinitis, conjunctivitis and excessive salivation and reduction in milk yield with depression, inappetence and emaciation [19,20].

Lab diagnosis of LSDV depends on isolation of the virus on the chorio-allantoic membrane (CAM) of 7-9 days old embryonated chicken eggs (ECEs) [21] or on tissue culture of bovine, caprine or ovine origin especially medin derby bovine kidney (MDBK) cell culture [10]. LSDV can be identified by transmission electron microscope and Histopathological examination that characterized by the presence of characteristic eosinophilic intracytoplasmic inclusion bodies [2,22]. The serum neutralization test (SNT) is the gold standard serological test for the determination of LSDV [23]. Enzyme-linked immunosorbent assay (ELISA) also permits rapid and simple serological detection of LSDV in serum samples [8]. Agar gel precipitation test (AGPT) and the fluorescence antibody test (FAT) also can be used for identification of LSDV [24,11]. Molecular detection of LSDV by means of polymerase chain reaction (PCR) and real-time PCR eliminates the technical, financial, and cost challenges associated with viral isolation and serological tests [25]. Real time PCR is quantitative, simpler, faster and more sensitive in comparison with conventional PCR [26].

A potential target for genetic discrimination between CaPV genus members is the G-protein-coupled chemokine receptor (GPCR) gene, which is involved in cell immunosuppression and proliferative lesions brought on by CaPV infections [27].

There is no specific treatment for LSDV but controlling of the virus depends on sanitary prophylaxis or vaccination programs using homologous live attenuated virus vaccine (Neethling strain vaccine) or heterologous live attenuated virus vaccine (Sheep or goat pox vaccine) [20]. For veterinary medicine, animal production, and other fields, nanotechnology holds out a lot of promise [28]. Due to their small sizes and substantial surface areas, nanoparticles (NPs) and their oxides, like zinc nanoparticles, have distinctive properties [29]. Attention has been drawn to the green synthesis of nanomaterials, which uses environmentally friendly techniques to create NPs without the use of hazardous chemicals and instead uses plant extracts, biomolecules, and ionic liquids in low-temperature processes **[30]**. Due to the virus's small size, the main goal of using nano-antivirals is to allow interactions between nanoparticles (NP), providing a practical treatment option **[31]**. Zinc oxide nanoparticles (ZnONPs) have been used as nanoparticles for

controlling and inhibiting of many viruses at *vitro* level including bovine herpesvirus-1 [30], H1N1 influenza virus [32], hepatitis C virus, hepatitis B virus [33] and Herpes Simplex Virus Type 1 (HSV-1) [34].

Due to the repeated occurrence of LSD in Egypt and due to its sever economic losses we aimed in this study to isolate the LSDV from samples, to make molecular characterization of the virus and to use ZnONPs as a promising antiviral agent against LSDV and inspect its effect at tissue culture level.

Material and Methods

Virological samples

Five skin nodule samples were collected form suspected cattle showing the clinical signs of LSD (as fever and nodules on skin) during August and September 2020 from five governorates in Egypt (Menofia, Beheira, Qalyubiya, Ismailia and Qena). These samples were labeled, transported and stored at -80 ºC (deep freezer) according to OIE [20] until be used for real time PCR, isolation, sequencing and application of antiviral nanomaterial.

Real time PCR for detection of LSDV

The five skin nodule samples were examined by real time PCR. The first step included preparation of samples and extraction of viral DNA from suspected prepared samples using (G-SPIN™ Total DNA Extraction Kit, Korea) according to the manufacturer instructions then the extracted DNA was stored at -20 ºC till be used. The second step, mix, was performed using commercial kit (LSDV dtec-qPCR test (GPS, Spain)). The content of the mixing kit was rehydrated and used according to the manufacturer instructions then applied to the real time PCR machine (Stratagene Mx3005P, Agilent, USA). The reaction was prepared in a sterile 0.2 ml tube. 20µl qPCR mix was prepared and mixed thoroughly by pipetting including 4µl mix stable qPCR 5x, 1µl specific primer/probe, 10 µl DNase/RNase free water and 5µl template (either sample, positive or negative). Positive control was supplied as a part of the mixing kit. Thermal profile, as described by manufacturer of the mixing kit, was adjusted to one cycle at 95°C for 15 min for (activation), followed by 40 cycles at 95°C for 15 sec for (denaturation) and 60°C for 1 min for (hybridization/extension and data collection). The cut off was at 35 cycle threshold (Ct) value as determined by the manufacturer.

Isolation of LSDV on CAM of SPF-ECEs

One positive skin nodule sample was selected to be isolated on chorioallantoic membrane (CAM) of specific pathogen free- embryonated chicken egg (SPF-ECE) [35]. The sample was prepared in phosphate buffered saline (pH 7.4) with 100 U/ml penicillin and 100 mg/ml streptomycin, After the homogenate was three times frozen and thawed to lyse the cells, the supernatant was purified by centrifuging at 6000 x g for five minutes at 4°C and was filtered through a 0.45 mm pore-size cellulose acetate filter. Before inoculation, the SPF-ECEs were incubated for 9 days at 37°C and 70% humidity. Then, they were injected with 0.2 ml of the supernatant through CAM after being incubated for 9 days [35]. Every day for seven days following inoculation, the ECEs were examined, and eggs that had died embryos within the first 24 hours after inoculation were regarded as non-specific deaths. Three passages of the virus in CAM were done to increase the virus titre. The result was confirmed by application of conventional PCR.

Sequencing and phylogenetic analysis

Detection of LSDV specific nucleic acid by conventional PCR

Conventional PCR was applied to detect nucleic acids of LSDV in the harvested CAM. The PCR amplification reaction was applied using AmpliTaq Gold™ 360 Master Mix (Applied Biosystems™ Thermo Fisher Scientific, Waltham, MA, USA) as per the manufacturer›s instructions. The PCR primers were produced by Bio Basic, Canada Inc. of Markham, Ontario, Canada, for the amplification of the partial sequence of GPCR gene that is specific for the LSDV. The primers were used to amplify a 554 bp fragment of the GPCR gene with primers sequences as follows: LSDVF (5›-AGT ACA GTT AGT AGC GCA ACC-3›) and LSDVR (5›-GGG TGA ACT ACA GCT AGG TAT C-3›) [36]. The PCR reaction total volume was 25 µl which was carried out using 6 µl of extracted DNA, 12.5 µl of 2x AmpliTaq Gold™ 360 Master Mix and 1 µl of 20 pmol of forward and reverse primers, the final volume was then reached using Nuclease-free water. The BIO-RAD® PCR system T100 thermocycler (BioRad, Hercules, California, USA) was preheated and set to the cycling protocol before DNA amplification was carried out. The cycling protocol included initial denaturation at 95°C for 10 mins followed by 40 cycles of: denaturation at 95°C for 60 sec., annealing at 50°C for 60 sec., and extension at 72°C for 60 sec., followed by final extension at

72°C 10 min. Positive and negative controls were included. According to Sambrook et al. [37], 1.5% agarose gel electrophoresis was used for evaluating the amplified PCR product. Molecular Imager Gel Doc™ XR+ Imaging system (BIO-RAD) was used to analyse gel images and identify the DNA band of predicted size in comparison to a 100 bp DNA molecular weight marker.

Viral DNA sequencing

The specific fragment of the GPCR gene in LSDV, measuring 554bp in size, was subjected to partial gene sequencing. The same primers and thermal profile used in the PCR were utilized for this sequencing process. The PCR reaction followed the previously described method, employing 2x AmpliTaq Gold™ 360 Master Mix. The resulting PCR amplicons were purified using the QIAquick® Gel Extraction Kit (Qiagen, Germany) according to the manufacturer instructions. The quantity and purity of the purified DNA was determined by spectrophotometry using the SPECTRO stars Nano (BMG LABTECH, Germany) and the absorbance was measured at 260nm and 280nm to determine concentration and purity. The purified DNA was used as template for Sanger sequencing with the BigDye Terminator v3.1 Cycle Sequencing Kit (Applied Biosystems, USA). CENTRI-SEP Spin Columns (PRINCETON SEPARATIONS, Inc., Adelphia, NJ, USA) were used to remove unincorporated dye terminators prior to sequencing based on the description by **[37]**. The purified products were resuspended in Hi-Di™ Formamide (Thermo Fisher Scientific, USA), denatured, and loaded onto the Applied Biosystems™ 3500 Series genetic analyzer system (Hitachi, Japan) at Anima Health Research Institute (AHRI). This capillary electrophoresis system automates sample injection, separation, and detection of fluorescently labeled DNA fragments.

Sequence alignment and phylogenetic analysis

The nucleotide sequence of the partial GPCR gene was submitted in the GeneBank under the name (LSD/204/EGYPT/MENOFIA/2020) with the accession number (OQ473500). Searching for GPCR nucleotide sequences of LSDVs was performed using the BLAST similarity search option in the GenBank database at the National Centre for Biotechnology Information in Bethesda, Maryland (available at http://www.ncbi.nlm.nih.gov). The selected GPCR coding domain sequences of LSDVs from GenBank, including the sequence obtained in this study, were used for phylogenetic analysis. Multiple sequence alignments of nucleotide sequences were performed using Bioedit with the ClustalW method [38]. Additionally, MEGA 7 software was utilized for phylogenetic analysis using the Neighbor-Joining method (NJ) following the approach described by [39].

Antiviral activity of ZnONPs against LSDV:-
Preparation and synthesis of green zinc oxide nanoparticles (ZnONPs): -

Arabic gum from the Acacia Senegal plant (AG) was purchased from a local market. Both sodium hydroxide (NaOH) and Zinc sulfate heptahydrate ($ZnSO_4$. $7H_2O$) were purchased from Sigma Aldrich, USA. The chemicals were all of analytical grade. All the synthesis process was carried out using deionized water. The ZnONPs were prepared by a green method using $ZnSO_4.7H_2O$ and NaOH as precursors at a molar ratio of 1:2 respectively and AG as stabilizing agent according to Geetha et al. [40] with a modification. A concentration of 1.5% AG (0.043 g) was prepared in 100 ml of deionized water. Then 2.88 g of $ZnSO_4.7H_2O$ was added to them to get 0.1 M solution. Using a magnetic stirrer, the mixture was continuously stirred to completely dissolve the zinc sulfate. NaOH (0.2 M, 0.8 g) was prepared in 100 ml deionized water, added dropwise, and stirring continued for 2 h, PH was adjusted to around 10. The solution was allowed to settle overnight then was centrifuged at 12000 rpm at 4 ºC for 30 min and The supernatant was removed. To remove the impurities, the obtained nanoparticles were washed three times with deionized water. For the full synthesis of ZnONPs, the nanoparticles were dried at 80 ºC for overnight in a hot air oven. The resulting clear white color powder was kept at room temperature for later use [40].

Nanomaterial characterization

The characterization of ZnONPs was carried out according to Melk et al. [34]. Using a NANOTRAC-WAVE II Zetasizer (MICROTRAC, USA), synthesised NPs' particle size and surface charge were evaluated. The phase identification and crystalline structure of the nanopowder were analyzed using X-ray diffraction (XRD) with Cu Ka radiation by X-ray Diffractometer (SHIMADZU, XRD-6000). The chemical composition and interaction between functional groups were detected by Fourier-transform infrared spectroscopy (FT-IR) (Perkin Elmer, UK) at scanning range of 4000-400 cm-1.

Transmission Electron Microscopy (TEM; JEM-2100, JEOL) was used to examine the morphology of synthesised NPs.

Determination of ZnONPs cytotoxicity on human oral epithelial cells (OEC)

were then incubated at room temperature (RT) in a darkened area for 10 min followed by washing with 1% acetic acid three times and allowed to dry in air. Then, 150 µl of TRIS buffer (10 mM) was used to dissolve SRB stain protein bounds. The absorbance was measured at 540 nm using a BMGLABTECH®- FLUOstar Omega microplate reader (Ortenberg, Germany).

Determination of CC50 of ZnONPs on MDBK tissue culture

Stock solutions of ZnONPs were created in 10% Dimethyl sulfoxide (DMSO) in distilled water and diluted further to the working solutions with DMEM to reach the half-maximal cytotoxic concentration (CC50). Using the crystal violet assay, ZnONPs' cytotoxic activity was assessed in Madin-Darby bovine kidney (MDBK) cells [42] using Ribavirin as a reference antiviral compound for comparison. The cells were plated in 96-well plates (100 µl/well at a density of 3×10^5 cells/ml), then were incubated for 24 h at 37 °C in 5% CO_2. Various concentrations of ZnONPs or ribavirin were administered to the cells in triplicates after 24 hours. After 72 hours, the supernatant was discarded, and cell monolayers were fixed with 10% formaldehyde for 1 hour at RT. Once fixed, the monolayers were thoroughly dried before being stained for 20 minutes at room temperature with 50 µl of 0.1% crystal violet. The monolayers were then washed, allowed to dry overnight, and the crystal violet dye in each well was dissolved in 200 µl of methanol for 20 min at RT. Using a multi-well plate reader, the absorbance of the crystal violet solutions was calculated at λmax 570 nm. By plotting the log concentrations of ZnONPs and ribavirin versus the normalized response (variable slope), nonlinear regression analysis was used to determine the CC50 value.

Determination of inhibitory concentration 50 of ZnONPs on LSDV in MDBK

The determination of IC50 of ZnONPs against LSDV was carried out following previously established protocols [42] using Ribavirin as a reference antiviral compound for comparison [33]. In each well of a 96-well tissue culture plate, 100 µl of MDBK cell suspension (3×10^5 cells) was added and incubated overnight in a humidified incubator at 37°C with 5% CO_2. The cell monolayers were then washed once with 1x Phosphate-buffered saline (PBS) and then subjected to LSDV adsorption for 1 hour at RT. The cell monolayers were overlaid with 50 µl of DMEM containing varying concentrations of ZnONPs or Ribavirin. After incubating for 72 hours at 37 °C in 5% CO_2, The cells were stained with 0.1% crystal violet in distilled water for 15 minutes at room temperature after being fixed with 100 µl of 4% paraformaldehyde for 20 minutes. The optical density of the color was then determined at 570 nm using an Anthos plate reader (BMGLABTECH®FLUOstar Omega, Germany) after the crystal violet dye had been dissolved using 100 µl of absolute methanol per well. Using GraphPad Prism software (version 5.01) and nonlinear regression analysis, the IC50 value was determined by plotting the logs of the concentrations of ZnONPs and ribavirin against the normalized response (variable slope).

TEM Analysis of the Antiviral Activity of ZnONPs against LSDV

TEM was used to explore the antiviral efficacy of ZnONPs against LSDV in MDBK tissue culture. As previously mentioned, the experimental procedure involved exposing the MDBK tissue culture to LSDV. The cell monolayer was then coated with 50 µl of DMEM that included 50 µg/ml of ZnONPs and it was incubated for 24 hours at 37 ºC within a 5% CO_2 environment. Afterwards, the samples were processed and examined according to Liu et al. **[43]** using a JEOL 1400 electron microscope (JEOL, Ltd., Japan) running at 80 Kv in comparison to positive infected MDBK cells by LSDV.

Results

Real time PCR

All tested samples by real time PCR were positive for LSDV (Table. 1) with different Ct between 18 and 23 values as presented in fig. (1). The cut off was at Ct 35 as determined by the manufacturer.

Isolation on CAM of SPF-ECEs

After three passages of the LSDV sample in CAM of SPF-ECEs, we demonstrated the presence of pock lesion, which is numerous, small, scattered opaque white foci in addition to congestion of blood in CAM blood vessels and turbidity of CAM as showed in **Fig (2)**. In each passage, a negative not inoculated control was included.

Sequencing and phylogenetic analysis

The isolated LSDV sample was examined by conventional PCR, using GPCR gene primers, and the result was positive with presence of band at 554 bp. The band was cut and purified for sequencing using DNA sequencer. The strain of the study LSD/204/EGYPT/MENOFIA/2020 **(OQ473500)** was aligned with other LSDV strains available in the GeneBank database by the ClustalW toll implemented in BioEdit software. The multiple alignment and phylogenetic analysis showed that the strain of the study segregated into LSDV group. It showed more than 99% identity with those strains of LSDV available in GeneBank. On comparing the field strain of the study with the Indian strains of 2019 as **(MW452639, MW452640 and MW452641)**, there was 12 nucleotide deletions in our strain from nucleotide number 94 to nucleotide number 105 of the entire gene. The phylogenetic analysis also showed that the stain of the study is closely related to the strains of LSDV of Africa and Middle East, which have the same 12 deletions as our strain **(Fig.3)**.

Antiviral activity of ZnONPs against LSDV
Characterization of ZnONPs

Particle size and zeta potential

According to Zetasizer's findings, ZnONPs have an average particle size of 67.8 nm and a narrow size distribution. polydispersity index (PDI) is 0.2 and surface charge of -25.7 mV **(Fig.4A)**.

X-ray diffraction

The XRD pattern of synthesized ZnONPs shown in **(Fig. 4B)**. Prominent peaks can be observed at 2θ of 18.80, 32.63, 37.68, 46.98, 58.35, 61.83 and 71.88°. The assignments of 2θ position and other parameters for ZnONPs from XRD were in agreement with the reference code (JCPDS file No. 80-0075) at wave length of 1.54060 with a hexagonal crystal system.

FT-IR Spectra

FT-IR spectra of synthesized Arabic gum and Zn NPs were shown in **(Fig.4C)**. For Arabic gum, the peak at 3500 cm^{-1} shows the presence of N-H bond in stretching mode, 3000 cm^{-1} show the presence of O-H bond stretching mode (carboxylic acid), 1600 cm^{-1} referred to the presence of N-H bond which bent in primary amine, 1430 cm^{-1} show the presence of C-O-H bond in bending mode, 1050 cm^{-1} show the presence of C-O bond in stretching mode and 600 cm^{-1} show the presence of C-l bond in stretching mode. For ZnONPs, N-H bond in stretching mode represented in the peak of 3430 cm^{-1}, 2923 cm^{-1} show the presence of O-H bond stretching mode (carboxylic acid), 1620 cm^{-1} referred to the presence of N-H bond which bent in primary amine, 1435 cm^{-1} show the presence of C-O-H bond in bending mode,1110 cm^{-1} show the presence of C-O bond in stretching mode and 420 cm^{-1} show the presence of C-l bond in stretching mode.

Morphological characters using TEM

ZnONPs were visualized using TEM images in **(Fig. 5.A1 and A2)**, which demonstrated distinct single NPs with spherical shape and no aggregation, with sizes ranging from 23.6 to 38.0 nm.

Determination of ZnONPs cytotoxicity on OEC

ZnONPs did not exhibit toxicity at concentrations lower than 50 mg/ml in the SRB assay for the cells incubated with them, and the cells maintained their original morphological characteristics when compared to control cells. According to **(Fig. 6)**, the survival rate dropped from 100.99 to 90.23 % at concentrations of 0.31 and 50 mg/ml, respectively.

Determination of CC50 of green synthesized ZnONPs on MDBK tissue culture and their effect on LSDV

The green synthesized ZnONPs have IC50 of 45.36 µg/ml against LSDV while they have CC50 of 30.90 µg/ml on MDBK tissue culture with selectivity index (SI) of 0.68 while Ribavirin has IC50 of 21.51 µg/ml against LSDV while it has CC50 of 10.60 µg/ml on MDBK tissue culture with SI of 0.5 **Fig (7)**.

TEM Analysis of the Antiviral Activity of ZnONPs against LSDV

TEM analysis of thin sections prepared from LSDV after incubation with 50 µg/ml of ZnONPs **(Fig.8 A-F)** revealed the adherence and accumulation of ZnONPs encircling the viral envelope, accompanied by protrusions. Furthermore, the viral particle displayed deformities, asymmetry, and shrinkage, along with the dispersion of NPs within the viral structure. Leakage of the internal contents occurred, resulting in an indistinct appearance of viral components. Both the viral envelope and capsid ruptured. Ultimately, the virus sustained extensive damage, leading to the emergence of a distinctive "Bite" appearance.

Discussion

Africa is experiencing an endemic spread of LSD, a serious disease that affects cattle and water buffalo **[27]**. The economic losses due to this disease are attributed to reduced milk production, loss of appetite and weight loss, poor growth, abortion, infertility, skin damage, and pneumonia, particularly in young animals **[9]**. Therefore, it is crucial to continue monitoring and inspecting the disease.

Natural infection with LSD provides lifelong immunity, and vaccination with live attenuated vaccines has been successfully used for disease control in endemic areas **[44]**. In this study, our focus was on the in *vitro* control of LSDV using nanoparticles as a novel approach.

The study involved the diagnosis of LSDV in nodular samples obtained from clinically infected cattle, followed by isolation on CAM of SPF-ECEs. Through sequencing, sequence analysis, and phylogenetic analysis using the GPCR gene, the virus molecular identity was determined.

Real time PCR is a sensitive, specific, qualitative and time saving technique for diagnosis of LSDV **[26]**. All five nodular samples tested positive for LSDV, with varying Ct values ranging from 18 to 23. This result is consistent with the findings of Helmy et al. **[25]**, which also used real-time PCR and detected the virus in 100% of nodular samples. These results highlight the efficacy of real-time PCR for identifying and detecting the causative agent of LSD.

One positive sample was isolated by inoculation in CAM of SPF-ECEs for three passages. The result revealed the presence of the specific pock lesion of *Poxviridae* in the form of numerous, scattered, small opaque white foci in addition to congestion of blood vessels of CAM, this result agreed with **[21,45,46]** whose results showed the same signs.

Subsequent steps in the study involved sequencing, sequence analysis, and phylogenetic analysis of the GPCR gene. GPCR gene likely influences cell proliferative lesions and immunosuppression during infections and was selected as a host discriminative gene for LSDV detection, as it contains a 21-nucleotide insertion and a 12-nucleotide deletion **[27]**. According to Gelaye et al. **[47]**, analysis of the GPCR gene sequence revealed significant differences between vaccine strains and field isolates. The high similarity between the nucleotide sequence of our strain's GPCR gene and those of LSDV strains circulating in Africa and the Middle East suggests that our strain is closely related to them. However, the presence of a 12-nucleotide deletion in our strain distinguishes it from the strains involved in the Indian outbreak of LSDV in 2019. This indicates that our strain may be a recombinant strain of LSDV, consistent with the findings of Sudhakar et al. **[48]**.

In our study, ZnONPs were synthesized by a green method using Arabic gum as stabilizing and capping agents. This method offers several advantages over other chemical methods, as it reduces environmental risks and avoids the use of hazardous components **[49]**. Surface modification of nanoparticles (NPs) plays a crucial role in controlling their morphological characteristics, particularly their size, to enhance their effectiveness and prevent NP agglomeration, which can hinder their application as antimicrobials **[50]**. Additionally, surface modification helps maintain electrostatic interactions and steric hindrance of NPs in a water system, relying on the polyanionic nature of Arabic gum **[51]**.

We utilized Arabic gum as a stabilizing and capping agent, with a ratio of 1.5%, along with sodium hydroxide as the precipitating agent for the synthesis of zinc oxide nanoparticles (ZnONPs). Arabic gum exudates possess hydrocolloid and emulsification properties and consist of a complex mixture of polysaccharides and glycoproteins, making it a multifunctional material with excellent stabilizing properties and biocompatibility, ensuring its non-toxic and safe nature **[52]**. Our method successfully synthesized ZnONPs with an average size of 67.8 nm and a narrow size distribution (PDI is 0.2). The surface charge of the synthesized ZnONPs was measured at 25.7 mV using a zetasizer **(Fig. 4A)**, and this finding was confirmed by TEM analysis **(Figs. 5.A1 and A2)**, which revealed distinct, well-dispersed ZnONPs with a spherical shape and no aggregation, ranging in size from 23.6 to 38.0 nm. It has been noted that using a lower amount of Arabic gum helps in forming a thin layer around ZnONPs, facilitating the adherence of smaller particles during the growth process when the NPs interact with functional groups of Arabic gum, such as carboxyl, hydroxyl, and amine groups, thereby preventing excessive growth **[53]**. Nanoparticles synthesized in the presence of Arabic gum as stabilizing agents usually

have negative charges on their surface **[54]**. The XRD pattern of the ZnONPs **(Fig.4B)** revealed characteristic peaks (marked by red) of the hexagonal phase of ZnONPs corresponding to 2θ values of 18.80, 32.63, 37.68, 46.98, 58.35, 61.83 and 71.88° at a wavelength of 1.54060 corresponding to reference code (JCPDS file No. 80-0075) as mentioned by **[55]**.

The role of Arabic gum in the synthesis of ZnONPs was identified by comparing the FT-IR **(Figs.4C)** of Arabic gum as stabilizing and capping agent with synthesized ZnONPs. For Arabic gum, specific peaks of N-H bond in stretching mode, O-H bond in stretching mode, N-H bond which bent in primary amine, and C-O bond in the stretching mode were observed at 3500, 3000, 1600, and 1050 cm^{-1} respectively compared with 3430, 2923, 1620 and 1110 cm^{-1} respectively for ZnONPs. The shifting in the peak of the N-H bond in the stretching mode of AG stabilized NPs compared with AG may be resulted from an interaction between AG protein and NPs while shifting in the peak of the C-O bond in the stretching mode of AG stabilized NPs compared with AG indicates new bond formation and as it was reported by Geetha et al. **[40]**. The higher shifting frequency is an indicator of structural changes related to binding between AG and NPs. The FT-IR study results further confirmed the successful role of Arabic gum in stabilizing ZnONPs.

Different factors impact the cytotoxicity of NPs especially shape, surface charge, size, surface modification and stabilization, and time-dose dependent effect which should be evaluated and kept in mind before application of NPs cytotoxicity in *vitro* or in *vivo* experimentation **[56]**. For ZnONPs, the primary mechanism of its cytotoxicity is the induction of oxidative stress and free radicals generation **[57]**. Our findings demonstrated the safety of the green synthesised ZnONPs by showing that the survival rate of OEC cell culture incubated with ZnONPs decreased from 100.99 to 90.23% by using concentrations of 0.31 to 50 mg/ml, respectively **(Fig. 6)**.

The relationship between surface functionalization of NPs using capping agents and nano cytotoxicity is closely related. It was reported that using long chain capping agents could reduce ROS generation and inhibit cytotoxicity even at high concentrations **[58]**. Arabic Gum as long chain polysaccharides used as capping and stabilizing agent in the synthesis of ZnONPs help in reducing cytotoxicity in a high concentration of less than 50 mg/ml due to controlling free radicals production and oxidative stress **[59]**. Conversely, ZnONPs exhibited cytotoxicity in the MDBK tissue culture at a concentration of 30.90 µg/ml after 72 hours of incubation. This outcome might be attributed to the specific characteristics of the cell culture and the duration of exposure to the NPs. **[60]** demonstrated that ZnONPs did not cause any significant toxicity at all concentrations during 24-hour and 48-hour exposures in MDBK and PK 15 cells. However, after 72 hours of exposure, cell viability significantly decreased.

ZnONPs have antiviral effect against several DNA and RNA viruses as Bovine herpes virus 1 **[30]**, influenza virus (H1N1) **[32]**, and hepatitis viruses **[33]**. The superiority and enhanced performance of ZnONPs compared to other antiviral metal oxide NPs can be attributed to their favorable compatibility with biological systems, affordability, high safety, and stability **[61]**. Our study demonstrated the antiviral effect of ZnONPs against LSDV at a concentration of 45.36 µg/ml. To the best of our knowledge, this is the first investigation to uncover the impact of Green synthesized NPs on LSDV as a DNA virus. Antiviral activity of metal-based nanoparticles depends on three mechanisms, (A) adhering to the virus and preventing it from attaching to and entering the cell; (B) destruction of the structure of viral proteins and function of viral nucleic acids due to the production of extremely active oxygen and other ions and radicals that stick to the wall (spikes or membrane); and (C) emulating the nucleus to boost the host cell's immune response and prevent the virus from budding and spreading **[62]**. ZnONPs' remarkable antimicrobial properties can be attributed to their increased specific surface area because the smaller particle size increases the reactivity of the particle surface **[63]**. Additionally, zinc ions selectively inhibit viral DNA polymerase, which prevents viral replication **[34]**.

TEM imaging revealed the promising efficacy of ZnONPs against LSDV, and to our knowledge, these are the first images illustrating the effect of ZnONPs on LSDV. TEM imaging demonstrated that ZnONPs can attach to the outer envelope of the virus which come in agreement with Gupta et al. **[33]** who demonstrated the ability of ZnONPs to adhere to the outer proteins of the virus, consequently hindering viral entry into cells. TEM imaging illustrated that ZnONPs

caused destruction of the outer envelope and other structural proteins of the virus, consistent with the findings of Jha et al. **[64]** who reported that ZnONPs generate numerous free radicals inducing oxidative stress, resulting in significant damage to viral membranes.

Conclusion

Our findings revealed that the LSDV strain we examined exhibited close similarities to strains found in Egypt, Middle East and Africa. However, significant differences were observed when compared to the strains identified during the 2019 outbreak in India. Therefore, it is suggested that the strain under investigation may represent a recombinant field strain. Consequently, further research and molecular characterization of LSDV are recommended to gain a better understanding of its epidemiology and genetic diversity. Furthermore, our findings represent a pioneering study that offers significant insights into the potential of ZnONPs as a highly promising antiviral agent against LSDV. This assertion is further corroborated by the conclusive evidence obtained from TEM imaging. The TEM imaging provided visual confirmation of the antiviral activity of ZnONPs, shedding light on the underlying mechanisms of action at the nanoscale level. This study stands as a crucial milestone in the exploration of ZnONPs efficacy against LSDV, paving the way for future research and the development of innovative antiviral strategies in *vivo*.

Conflict of interest

The authors certify that they are free of any conflicts of interest.

Funding statement

Not applicable, as There were no funding resources and the authors did this work by themselves without any funding.

TABLE 1. Samples details and Ct values of real time PCR

Sample no.	Governorate	Sample type	Ct value
1	Menofia	Skin nodule	18
2	Beheira	Skin nodule	19
3	Qalyubiya	Skin nodule	21
4	Ismailia	Skin nodule	23
5	Qena	Skin nodule	23

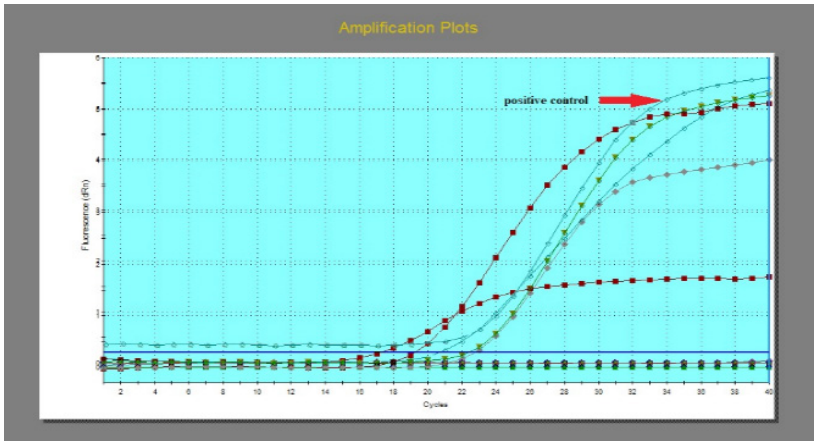

Fig. 1. Multicomponent plot of real time PCR with Ct values 18:23.

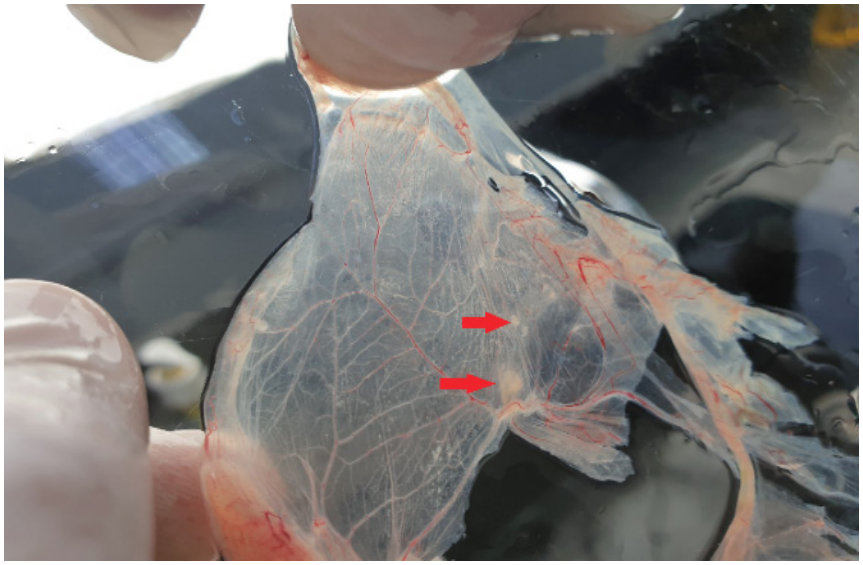

Fig. 2. LSDV lesion on CAM of SPF-ECE varied form congestion of blood vessels, turbidity of the membrane and presence pock lesion (red arrows).

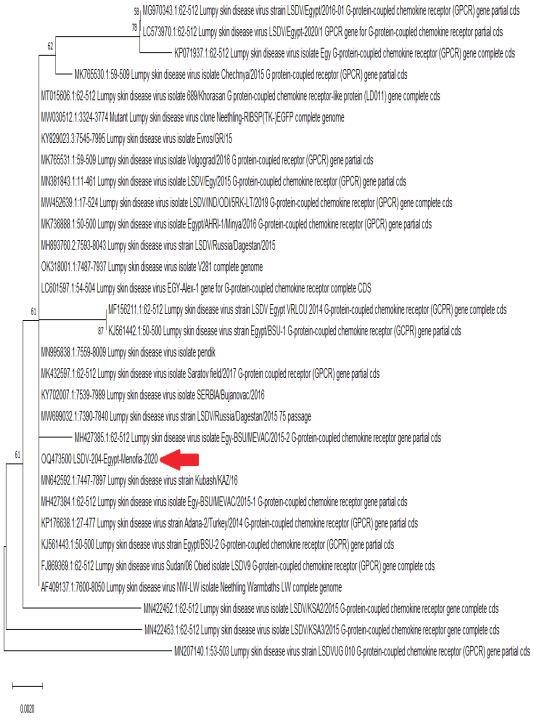

Fig. 3. Neighbor-joining phylogenetic tree constructed using the sequence of GPCR gene of LSDV, showing the relationship between LSDV strain of the study (LSD/Menofia/2020/GPCR gene) (red arrow) and LSDV strains available in GeneBank database using MEGA 7 software using Neighbor-joining (ML) statistical method. The reliability of each tree branch was calculated using 1000 bootstrap replicates.

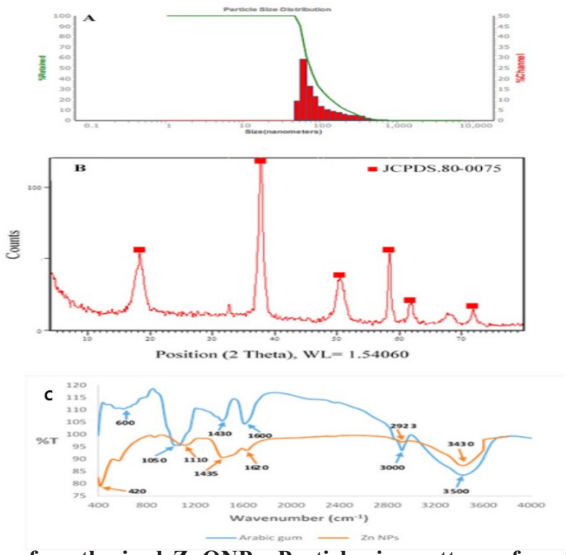

Fig.4. Characterization of synthesized ZnONPs. Particle size pattern of synthesized NPs showing (A) average particle size of ZnONPs of 67.8 nm and PDI (0.2). (B) XRD pattern of ZnONPs at the wavelength of 1.54060. (C) FT-IR spectra of ZnONPs at the scanning range of 4000-400 cm^{-1} compared with Arabic gum.

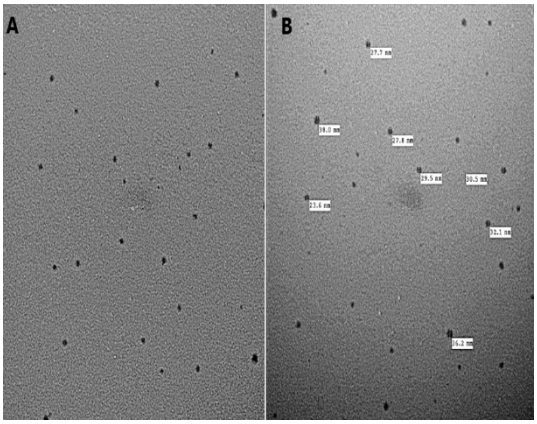

Fig.5. Morphological characters of synthesized ZnONPs, (A and B) by Transmission Electron Microscopy (TEM) imaging. The chosen field displayed spherical nanoparticles that were evenly dispersed and ranged in size from 23.6 to 38.0 nm (scale bar: 100 nm).

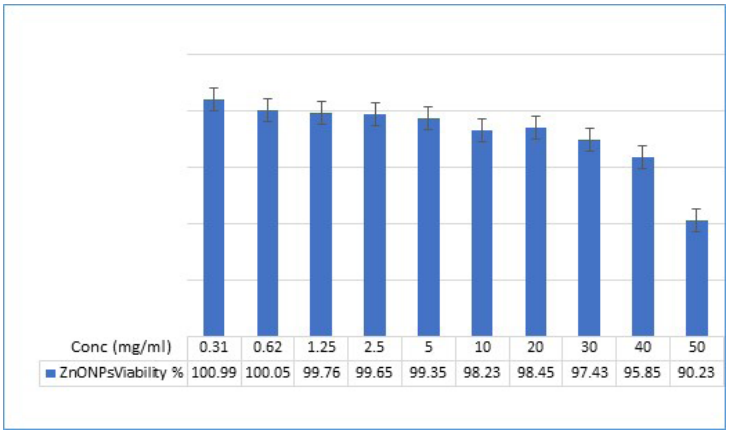

Fig.6. Sulforhodamine B (SRB) cytotoxicity assay of ZnONPs on human oral epithelial cells (OEC) tissue culture at different concentrations ranged from 0.31 to 50 mg/ml.

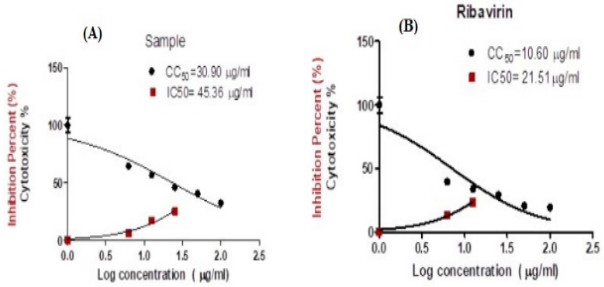

Fig.7. (A) The black line represents the cytotoxicity effect (CC_{50}) of ZnONPs on Madin Darby Bovine kidney (MDBK) and the red line represents the antiviral effect (IC_{50}) of ZnONPs against LSDV. (B) The black line represents the cytotoxicity effect (CC50) of Ribavirin on Madin Darby Bovine kidney (MDBK) and the red line represents the antiviral effect (IC_{50}) of Ribavirin against LSDV. By using nonlinear regression analysis, each graph was created. Each graph showed the log concentrations against the normalized response for cell viability.

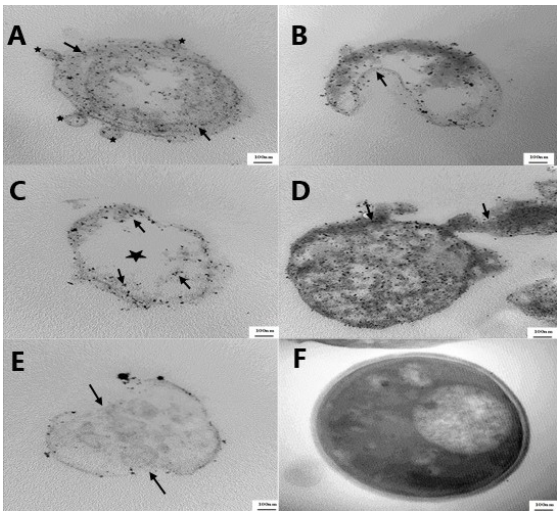

Fig. 8. TEM images of LSDV after incubation with 50 µg/ml of ZnONPs. (A) Showed accumulation of nanoparticles on viral envelope (arrows) with protrusions (stars) and penetration of nanoparticles. (B) Showed deformity and asymmetry of the viral particle (arrow). (C) Showed distribution of ZnONPs inside the viral particle (arrows) with lacking of viral content (star). (D) Rupture viral envelope and capsid with releasing of internal contents to outside (arrows). (E) Bite appearance (arrows) and complete viral damage 24 hours post incubation compared with intact viral positive control (F). Scale bar = 100 nm.

References

1. Kara, P. D., Afonso, C. L., Wallace, D. B., Kutish, G. F., Abolnik, C., Lu, Z., Vreede, F. T., Taljaard, L. C. F., Zsak, A., Viljoen, G. J and Rock, D. L.'Comparative sequence analysis of the South African vaccine strain and two virulent field isolates of Lumpy skin disease virus. *Archives of Virology*, **148** (7), 1335–1356(2003)**.** doi: 10.1007/s00705-003-0102-0.

2. Coetzer, J. and Tuppurainen, E. Lumpy skin disease, *Oxford University Press Southern Africa*, **2**, pp. 1269–1276(2004).

3. Tuppurainen, E. S. M. and Oura, C. A. L. 'Review: Lumpy Skin Disease: An Emerging Threat to Europe, the Middle East and Asia', *Transboundary and Emerging Diseases*, **59**(1), pp. 40–48. (2012)**.** doi: 10.1111/j.1865-1682.2011.01242.x.

4. Abera, Z., Degefu, H., Gari, G. and Kidane, M. 'Review on Epidemiology and Economic Importance of Lumpy Skin Disease', *International Journal of Basic and Applied Virology*, **4**(1), 8–21(2015). doi: 10.5829/idosi.ijbav.2015.4.1.9117.

5. Awad, W. S., Ibrahim, A. K., Mahran, K., Fararh, K. M and Abdel Moniem, M. I. Evaluation of different diagnostic methods for diagnosis of Lumpy skin disease in cows. *Tropical Animal Health and Production*, **42**(4), 777–783. (2010) doi: 10.1007/s11250-009-9486-5.

6. Abdel-rahim, I. H. A., Elballal, S. and Hussein, M. An outbreak of Lumpy skin Disease among cattle in Upper Egypt. *Minufyia Veterinary Journal,* **2**(1), 185-200 (2002).

7. Abd-EL-Hady, A.A.A. A field Study on Lumpy Skin Disease. *Assuit, Veterinary Medical Journal,* **52(**109)*,* 215-223(2006).

8. Möller, J., Moritz, T., Schlottau, K., Krstevski, K., Hoffmann, D., Beer, M. and Hoffmann, B. Experimental lumpy skin disease virus infection of cattle: comparison of a field strain and a vaccine strain. *Archives of Virology*, **164**(12), 2931–2941 (2019). doi: 10.1007/s00705-019-04411-w.

9. Abdulqa, H.Y., Rahman, H.S., Dyary, H.O. and Othman*.* H.H. Lumpy Skin Disease. *Journals Reproductive Immunology*, **1**(2), 1–6 (2016). doi: 10.3823/083.

10. El-Desawy, O. M. Recent Isolation and identification of lumpy skin disease virus from cattle in Egypt. *Egypt. J. Pathol. Clin. Pathology*, **21** (1), 139–147(2008).

11. Tuppurainen, E.S., Venter, E.H. and Coetzer, J. A. The detection of lumpy skin disease virus in samples of experimentally infected cattle using different diagnostic techniques The detection of lumpy skin disease virus in samples of experimentally infected cattle using different diagnostic techniques. *Onderstepoort Journal of Veterinary Research*, **72**(2), 153–164 (2005).

12. Tulman, E.R., Afonso, C.L., Lu, Z., Zsak, L., Kutish, G.F. and Rock, D.L. Genome of Lumpy Skin Disease Virus Genome of Lumpy Skin Disease Virus. *Journal of Virology*, **15**, 7122–7130(2001). doi: 10.1128/JVI.75.15.7122

13. Le Goff, C., Lamien, C. E., Fakhfakh, E., Chadeyras, A., Aba-Adulugba, E., Libeau, G., Tuppurainen, E., Wallace, D. B., Adam, T., Silber, R., Gulyaz, V., Madani, H., Caufour, P., Hammami, S., Diallo, A and Albina, E. Capripoxvirus G-protein-coupled chemokine receptor: A host-range gene suitable for virus animal origin discrimination. *Journal of General Virology*, **90**(8), 1967–1977(2009). doi: 10.1099/vir.0.010686-0.

14. Shalaby, M. A., El-Deeb, A., El-Tholoth, M., Hoffmann, D., Czerny, Cl., Hufert, F. T., Weidmann, M. and Abd El Wahed, A. Recombinase polymerase amplification assay for rapid detection of lumpy skin disease virus. *BMC Veterinary Research*, **12**, 244 (2016). doi: 10.1186/s12917-016-0875-5

15. Chihota, C. M., Rennie, L. F., Kitching, R. P and Mellor, P. S. Mechanical transmission of lumpy skin disease virus by Aedes aegypti (Diptera: Culicidae). *Epidemiology and Infection*, **126**(2), 317–321 (2001). doi: 10.1017/S0950268801005179.

16. Lubinga, J. C., Tuppurainen, E. S. M., Coetzer, J. A. W., Stoltsz, W. H and Venter, E. H. Evidence of lumpy skin disease virus over-wintering by transstadial persistence in Amblyomma hebraeum and transovarial persistence in Rhipicephalus decoloratus ticks. *Experimental and Applied Acarology*, **62**(1), 77–90 (2014). doi: 10.1007/s10493-013-9721-7.

17. Irons, P. C., Tuppurainen, E. S. M. and Venter, E. H. Excretion of lumpy skin disease virus in bull semen. **63**, 1290–1297 (2005). doi: 10.1016/j.theriogenology.2004.06.013.

18. Haftu, R. G. B. Lumpy Skin Disease (Lsd): Outbreak Investigation, Isolation and Molecular Detection of Lsdv in Selected Areas of Eastern Shewa, Ethiopia. *PhD Proposal*, **1**, 1–65. (2012). doi: 10.1017/CBO9781107415324.004.

19. Wainwright, S., El Idrissi, A., Mattioli, R., Tibbo, M., Njeumi, F. and Raizman, E. Emergence of lumpy skin disease in the Eastern Mediterranean Basin countries. *Empres Watch*, **29**, 1-6 (2013).

20. OIE **(**World Organization for Animal Health). "Lumpy skin disease," *OIE Terr. Anim. Heal. Code*, May, pp. 1–4, (2010), doi: 10.1007/BF02239636..

21. El-Bagoury, G., El-Nahas, E.M., Helmy, N.M. and Elhamady, M.G. Recent isolation and identification of a lumpy skin disease virus from Qaluobia Province, Egypt 2016. *Benha Veterinary Medical Journal*, **34**(1), 484–488 (2018).

22. Salib, F. A. and Osman, A. H. 'Incidence of lumpy skin disease among Egyptian cattle in Giza Governorate, Egypt', *Veterinary World*, **4**(4), pp. 162–167. doi: 10.5455/vetworld.2011.162-167. (2011).

23. Babiuk, S., Wallace, D. B., Smith, S. J., Bowden, T. R., Dalman, B., Parkyn, G., Copps, J and Boyle, D. B. 'Quantification of lumpy skin disease virus following experimental infection in cattle', *Transboundary and Emerging Diseases*, **55**(7), pp. 299–307. (2008). doi: 10.1111/j.1865-1682.2008.01024.x.

24. Amal, M. A., Raof, Shahein, M. A. and Hoda, A. E. M. 'Electrophoretic characterization of sheep pox virus, Goat pox virus and lumpy skin disease virus', *Egypt. J. Comp. Path. & Clinic. Path.*, **21**(1), pp. 15–30. (2008).

25. Helmy, N.M., Ahmed, A.S. and Mohamed, Z. Y. 'Molecular , clinico-pathological and sero-diagnosis of LSDV in cattle at Sharkia and Fayoum Governorates', *Journal of Virological sciences*, **1**(2001), 1–11. (2017)

26. Vidanović, D., Šekler, M., Petrović, T., Debeljak, Z., Vasković, N., Matović, K. and Hoffmann, B. Real-Time PCR Assays for the Specific Detection of Field Balkan Strains of Lumpy Skin Disease Virus. *Acta Veterinaria*, **66**(4), 444-454 (2016). doi: 10.1515/acve-2016-0038.

27. El-Tholoth, M. and El-Kenawy, A. A. G-Protein-Coupled Chemokine Receptor Gene in Lumpy Skin Disease Virus Isolates from Cattle and Water Buffalo (Bubalus bubalis) in Egypt. *Transbound. Emerg. Dis.*, **63**(6) 288–295(2016). doi: 10.1111/tbed.12344.

28. Nagajyothi, P., Deyarayapalli, K. C., Tettey, C. O., Prabhakar Vattikuti, S. V. and Shim, J. Eco-friendly green synthesis: Catalytic activity of nickel hydroxide nanoparticles. *Mater. Res. Express*, **6**(5), 055036 (2019). doi: https://doi.org/10.1088/2053-1591/ab04e4 Manuscript.

29. Jeevanandam, J., Barhoum, A., Chan, Y. S., Dufresne, A. and Danquah, M. K. Review on nanoparticles and nanostructured materials: history, sources, toxicity and regulations. *BEILSTEIN J. Nanotechnol.*, **9**(1), 1050–1074(2018). doi: https://doi.org/10.3762/bjnano.9.98.

30. Zeedan, G. S.G., Abd El-RaZiK, K. A., Allam, A. M., Abdalhamed, A. M. and Abou Zeina, H. A. Evaluations of Potential Antiviral Effects of Green Zinc Oxide and Silver Nanoparticles against Bovine Herpesvirus-1. *Adv. Anim. Vet. Sci.*, **8**(4), 433–443(2020).

31. Innocenzi, P. and Stagi, L. Carbon-based antiviral nanomaterials: Graphene, C-dots, and fullerenes. A perspective. *Chem. Sci.*, **11** 6606–6622(2020).

32. Ghaffari, H., Tavakoli, A., Moradi, A., Tabarraei, A., Bokharaei-Salim, F., Zahmatkeshan, M., Farahmand, M., Javanmard, D., Kiani, S. J., Esghaei, M., Pirhajati-Mahabadi, V., Monavari, S. H and Ataei-Pirkooh, A. Inhibition of H1N1 influenza virus infection by zinc oxide nanoparticles: another emerging application of nanomedicine Hadi. *Journal of Biomedical Science*, **26**(70), 1–10. (2019).

33. Gupta, J., Irfan, M., Ramgir, N., Muthe, K. P., Debnath, A. K., Ansari, S., Gandhi, J., Ranjith-Kumar, C. T and Surjit, M. Antiviral Activity of Zinc Oxide Nanoparticles and Tetrapods Against the Hepatitis E and Hepatitis C Viruses. *Frontiers in Microbiology*, **13**, 881595. pp. 1-14(2022). doi: 10.3389/fmicb.2022.881595.

34. Melk, M. M., El-Hawary, S. S., Melek, F. R., Saleh, D. O., Ali, O. M., EL Raey, M. A and Selim, N. M. Antiviral Activity of Zinc Oxide Nanoparticles Mediated by Plumbago indica L. Extract Against Herpes Simplex Virus Type 1 (HSV-1). *International Journal of Nanomedicine*, **16**, 8221–8233 (2021). doi: 10.2147/IJN.S339404.

35. House, J.A.,Wilson, T.M., El Nakashly, S., Karim, I.A., Ismail, I.,El Danaf, N., Moussa, A.M. and Ayou, N.N. The isolation of lumpy skin disease virus and bovine herpesvirus- from cattle in Egypt. *J. Vet. Diagn. Invest*., **2**, 111-115 (1990).

36. Mashaly, M. M., El-Deeb, A. H., Shahein, M. A. and Hussein, H. A. Molecular Characterization and cytopathogenecity of lumpy skin disease virus in Egypt. [master's thesis, Faculty of Veterinary Medicine, Cairo University, Egypt]. (2020).

37. Sambrook, J., Fritsch E. F., and Maniatis, T. Molecular cloning. *A laboratory Manual,* (2nd edn). Cold Spring Harbour Laboratory Press, New York. (1989).

38. Hall, T. A. BioEdit: a user-friendly biological sequence alignment editor and analysis program for Windows 95/98/NT. in *Nucleic acids symposium series*. [London]: Information Retrieval Ltd., c1979-c2000., pp. 95–98(1999).

39. Kumar, S., Stecher, G. and Tamura, K. MEGA7: molecular evolutionary genetics analysis version 7.0 for bigger datasets. *Molecular Biology and Evolution*, **33**(7), 1870–1874(2016).

40. Geetha, A., Sakthivel, R., Mallika, J., Kannusamy, R. and Rajendran, R. Green Synthesis of Antibacterial Zinc Oxide Nanoparticles Using Biopolymer Azadirachta indica Gum. *Oriental Journal of Chemistry* , **32**(2), 955–963 (2016).

41. Allam, R. M., Al-Abd, A. M., Khedr, A., Sharaf, O. A., Nofala, S. M., Khalifa, A. E., Moslie, H. A and Abdel-Naim, A. B. Fingolimod interrupts the cross talk between estrogen metabolism and sphingolipid metabolism within prostate cancer cells Authors. *Toxicology Letters*, **291**, 77–85 (2018). doi: 10.1016/j.toxlet.2018.04.008.

42. AbouAitah, K., Allayh, A. K., Wojnarowicz, J., Swiderska-Sroda, A. and Lojkowski, W. Nanoformulation Composed of Ellagic Acid and Functionalized Zinc Oxide Nanoparticles Inactivates DNA and RNA Viruses. *Pharmaceutics*, **13**(12), 2174–2191 (2021).doi: 0.3390/pharmaceutics13122174.

43. Liu, Y., He, L., Mustapha, A., Li, H., Hu, Z.Q., and Lin, M. Antibacterial activities of zinc oxide nanoparticles against Escherichia coli O157:H7. *Journal of Applied Microbiology*, **107**(4), 1193–1201(2009).

44. Hailu, B. and Alemayehu, G. Economic Importance and Control Techniques of Lumpy Skin Diseases. *Animal and Veterinary Sciences*, **3**(2), 58–66 (2015). doi: 10.11648/j.avs.20150302.15.

45. El-Kady, G. HE. M., El-Bagoury, G. F., El-Nahas, E. M and El-Habbaa, A. S. A Phylogeny of Envelope protein like gene of Lumpy skin disease virus , Egypt , 2014. *Benha Veterinary Medical Journal*, **4**(3), 338–354 (2018).

46. El-Habbaa, A., Abd-Elhafeez, S.N., El-mayet, F.S., Ateya, L.A. and El-Nahas, E.M. Molecular detection and phylogenetic analysis of ORF103 and P32 genes of Capripoxviruses isolated from naturally infected cattle and sheep from Kaliobyia province in Egypt. *Benha Veterinary Medical Journal*, **41**(1), 45–50 (2021).

47. Gelaye, E., Belay, A., Ayelet, G., Jenberie, S., Yami, M., Loitsch, A., Tuppurainen, E., Grabherr, R., Diallo, A. and Lamien, C. E. Capripox disease in Ethiopia: Genetic differences between field isolates and vaccine strain, and implications for vaccination failure. *Antiviral Research*, **119**,28–35(2015).

48. Sudhakar, S.B., Mishra, N., Kalaiyarasu, S., Jhade, S.K. and Singh, V.P. Genetic and phylogenetic analysis of lumpy skin disease viruses (LSDV) isolated from the first and subsequent field outbreaks in India during 2019. *Transboundary and Emerging Diseases*, **69**(4), e451–e462 (2022). doi: 10.1111/tbed.14322.

49. Sebeia, N., Jabli, M. and Ghith, A. Biological synthesis of copper nanoparticles, using Nerium oleander leaves extract: Characterization and study of their interaction with organic dyes Nouha. *Inorganic Chemistry Communications*, **105**, 36–46(2019).doi: 10.1016/j.inoche.2019.04.023.

50. El-Batal, A. I., Mosalam, F. M., Ghorab, M. M., Hanora, A. and Elbarbary, A. M**.** Antimicrobial, Antioxidant and Anticancer Activities of Zinc Nanoparticles Prepared by Natural Polysaccharides and Gamma Radiation. *Ternational Journal of Biological Macromolecules*, **107**, 2298–2311(2018).

51. Barros, H. R., Cardoso, M. B., Oliveira, C. C., Franco, C. R. C., Belan, D. L., Vidottia, M and Riegel-Vidotti, I. C. Stability of gum arabic-gold nanoparticles in physiological simulated pHs and their selective effect on cell lines. *RSC Advances*, **6**, 9411–9420. (2016). doi: 10.1039/c5ra24858b.

52. Daoub, R. M. A., Elmubarak, A. H., Misran, M., Hassan, E. A and Osman, M. E. Characterization and functional properties of some natural Acacia gums. *Journal of the Saudi Society of Agricultural Sciences*, **17**(3), 241–249 (2016). doi: 10.1016/j.jssas.2016.05.002.

53. BA-Abbad, M. M., Takriff, M. S. and Benamor, A. Arabic gum as green agent for ZnO nanoparticles synthesis : properties , mechanism and antibacterial activity', *Journal of Materials Science: Materials in Electronics*, **28**(16), 12100–12107(2017). doi: 10.1007/s10854-017-7023-2.

54. Chawla, P., Kumar, N., Bains, A., Dhull, S. B., Kumar, M., Kaushik, R and Punia, S. Gum arabic capped copper nanoparticles: Synthesis, characterization, and applications. *International Journal of Biological Macromolecules*, **146**, 232–242 (2020). doi: 10.1016/j.ijbiomac.2019.12.260.

55. Arora, A. K., Devi, S., Jaswal, V. S., Singh, J., Kinger, M and Gupta, V. D. Synthesis and Characterization of ZnO Nanoparticles. *Oriental Journal of Chemistry* , **30**(4), 1671–1679(2014). doi: 10.13005/ojc/300427.

56. Naz, S., Gul, A. and Zia, M. Toxicity of copper oxide nanoparticles : a review study. *IET Nanobiotechnology*, **14**(1), 1–13 (2020). doi: 10.1049/iet-nbt.2019.0176.

57. Pandurangan, M. and Kim, D. H. In vitro toxicity of zinc oxide nanoparticles : a review. *Journal of Nanoparticle Research*, **17**, 158(2015). doi: 10.1007/s11051-015-2958-9

58. Shi, M., Kwon, H. S., Peng, Z., Elder, A. and Yang, H. Article effects of Surface Chemistry on the Generation of Reactive Oxygen Species by Copper Nanoparticles. *ACS Nano*, **6**(3), 2157-2164 (2012). doi: 10.1021/nn300445d.

59. Prasad, P. R., Kanchi, S. and Naidoo, E. In-vitro evaluation of copper nanoparticles cytotoxicity on prostate cancer cell lines and their antioxidant, sensing and catalytic activity: One-pot green approach', *Journal of Photochemistry and Photobiology B: Biology*, **161**, 375–382(2016). doi: 10.1016/j.jphotobiol.2016.06.008.

60. Saranya, S., Vijayaranai, K., Pavithra, S., Raihana, N. and Kumanan, K. 'In vitro cytotoxicity of zinc oxide, iron oxide and copper nanopowders. *Toxicology Reports*, **24**(4),427–430(2017). doi: 10.1016/j.toxrep.2017.07.005.

61. Jiang, J., Pi, J. and Cai, J. The Advancing of Zinc Oxide Nanoparticles for Biomedical Applications. *Bioinorganic Chemistry and Applications,* **2018**, Article ID 1062562, PP. 1-18(2018). doi: 10.1155/2018/1062562

62. Zhou, J., Hu, Z., Zabihi, F., Chen, Z. and Zhu, M. Progress and Perspective of Antiviral Protective Material. *Advanced Fiber Materials*, **2**(3), 123-139(2020). doi: 10.1007/s42765-020-00047-7.

63. Hassan, H. S. Abol-Fotouh, D., Salama, E and Elkady, M. F. Assessment of antimicrobial , cytotoxicity , and antiviral impact of a green zinc oxide / activated carbon nanocomposite. *Scientific Reports*, **12** (8774), 1–12(2022). doi: 10.1038/s41598-022-12648-w.

64. Jha, S., Rani, R. and Singh, S. Biogenic Zinc Oxide Nanoparticles and Their Biomedical Applications: A Review. *J. Inorg. Organomet. Polym,* Springer US, (2023). doi: 10.1007/s10904-023-02550-x

جسيمات أكسيد الزنك النانوية: علاج مضاد للفيروسات واعد لفيروس مرض الجلد العقدي في المختبر.

جبر فكري الباجورى[١]، عصام إسماعيل الطوخي[٢]، محمد جمال الحمادي[٢] وسمر قاسم[٣]

[١] قسم الفيرولوجيا، كلية الطب البيطري، جامعة بنها.

[٢] قسم البيوتكنولوجى، معهد بحوث الصحة الحيوانية، الدقي، مركز البحوث الزراعية، الجيزة، مصر.

[٣] وحدة بحوث وتصنيع المواد النانوية، معهد بحوث الصحة الحيوانية، الدقي، مركز البحوث الزراعية، الجيزة، مصر.

تم جمع خمس عينات عقدية من الأبقار المشتبه إصابتها سريريًا بمرض الجلد العقدي من خمس محافظات في مصر خلال أغسطس وسبتمبر ٢٠٢٠. أكد تفاعل إنزيم البلمرة المتسلسل ذو الوقت الحقيقي وجود فيروس الجلد العقدي في جميع العينات. تم عزل عينة واحدة لثلاث مرات على غشاء المشيمي لأجنة الدجاج النامية الخالية من مسببات الأمراض المحددة، مما أدى إلى تشكل الأثر الباثولوجي المميز لفيروس مرض الجلد العقدي والذي يتميز بظهور عدد من البؤر البيضاء التنكرزية مما كشف عن ارتباطها الوثيق بسلالات فيروس الجلد ،GPCR المتناثرة. خضعت العينة المعزولة لتسلسل جزئي للجين العقدي المتداولة في أفريقيا والشرق الأوسط. لاحقًا، تم تصنيع جسيمات الزنك النانوية باستخدام طريقة خضراء باستخدام كبريتات الزنك سباعي الهيدرات (هيبتاهيدرات) كسلف لجزيئات الزنك النانوية وتم استخدام الصمغ العربي كعامل تثبيت. حيود ،(Zetasizer) وجهاز قياس الحجم ،(FT-IR) أظهر توصيف جسيمات الزنك النانوية باستخدام مطيافية تحول فوريه والمجهر الإلكتروني النافذ نطاق حجم من ٢٣,٦ إلى ٣٨,٠ نانومتر وشحنة سطحية سالبة تعادل ، (XRD)الأشعة السينية ٢٥,٧ مللي فولت. تم تقييم سمية جسيمات الزنك النانوية على خلايا الظهارة الفموية البشرية، مما أظهر أن معدل البقاء على قيد الحياة للخلايا انخفض من ١٠٠,٩٩٪ إلى ٩٠,٢٣٪ عند تركيزات ٠,٣١ و٥٠ ملغ / مل على التوالي. تم استخدام جسيمات الزنك النانوية لتثبيط تكاثر فيروس الجلد العقدي في خلايا كلى الأبقار الجنينية مادين داربي المزروعة باستخدام اختبار تخفيض اللويحة، مما أظهر تركيز تثبيط ٥٠٪ عند ٤٥,٣٦ ميكروغرام / مل وسمية خلوية عند ٣٠,٩ ميكروغرام / مل مع مؤشر انتقائية ٠,٦٨. علاوة على ذلك، أكد تصوير المجهر الإلكتروني النافذ الفعالية المضادة للفيروسات لجسيمات الزنك النانوية ضد فيروس الجلد العقدي. توضح هذه النتائج التأثير المضاد للفيروسات لجسيمات الزنك النانوية ضد فيروس الجلد العقدي، مما يوفر تطبيقات واعدة في مجال الطب البيطري.

الكلمات الدالة: فيروس مرض الجلد العقدي، تفاعل انزيم البلمرة المتسلسل ذو الوقت الحقيقي، جين ال GPCR، مضاد الفيروسات، جزيئات الزنك أوكسيد النانوية.